Available online at www.sciencedirect.com

jmr&t Journal of Materials Research and Technology

www.jmrt.com.br

Original Article

Nanoscale precipitates evolution and strengthening mechanism of the aged Cu-Mg-Fe-Sn-P-Y electrical contact wire

Bingjie Wang[a,b], *Yi Zhang*[a,b,*], *Baohong Tian*[a,b], *Yanlin Jia*[c,*], *Alex A. Volinsky*[d], *Vladislav Yakubov*[d], *Yong Liu*[a,b], *Kexing Song*[a,b], *Ming Fu*[e]

[a] *School of Materials Science and Engineering, Henan University of Science and Technology, Luoyang 471023, PR China*
[b] *Collaborative Innovation Center of Nonferrous Metals, Henan Province, Luoyang 471023, PR China*
[c] *School of Materials Science and Engineering, Beijing University of Technology, Beijing 100124, PR China*
[d] *Department of Mechanical Engineering, University of South Florida, Tampa 33620, USA*
[e] *Luoyang Electro-Optics Technology Development Centre, Luoyang 471023, PR China*

ARTICLE INFO

Article history:
Received 13 October 2019
Accepted 13 March 2020
Available online 18 May 2020

Keywords:
Aging treatment
Nanoscale precipitate
Dispersion strengthening
Orientation relationship

ABSTRACT

The evolution and strengthening effect of nanoscale precipitates of the aged Cu-Mg-Fe-Sn-P-Y alloy were investigated via aging treatment in the 400–480 °C temperature range and the 10–480 min aging time range. Nanoscale γ-Fe particles uniformly distributed in the matrix caused dispersion strengthening in the peak-aging stage and transformed to α-Fe at the over-aging stage. The Mg_3P_2 secondary phase hindered the appearance of coarse Fe_3P and formed definite orientation relationship (OR) of cubic to cubic with the Cu matrix after 480 min aging, $<110>_{Cu}||<110>_{Mg3P2}$, $(002)_{Cu}||(008)_{Mg3P2}$. The optimal aging parameter for the Cu-Mg-Fe-Sn-P-Y alloy is 60% cold deformation and aged at 460 °C for 20 min. The corresponding tensile strength is 599 MPa with the conductivity of 71.1%IACS and the elongation of 6.9%. Compared with the current contact wire, the ultimate tensile strength and conductivity of the studied alloy increased by 20% and 15%, respectively.

1. Introduction

Cu-Mg alloys are one of the upmost conductive materials used as contact wires, given in their excellent conductivity and superior strength, compared with Cu-Sn and Cu-Cd alloys. At present, Cu-Mg alloys are widely used in electrical contact lines for above 350 km/h in high-speed trains in China, which are almost the fastest high-speed trains in the world. The maximum train speed using Cu-Sn wires is 300–350 km/h, and 210 km/h for the Cu-Cd alloys [1–3]. Due to the high speed of the train, perfect performance of the Cu-Mg alloy contact wire is required. However, due to the poor fluidity and hot working performance of the Cu-Mg alloy, continuous casting and rolling (CCR) cannot be used for production. Thus, numerous investigations have focused on the equal channel angular pressing (ECAP) and high-pressure torsion (HPT) to reduce the stacking fault energy and improve the strength and plasticity of the materials. The above methods mainly emphasize the deformation behavior and the role of

* *Corresponding authors.*
E-mails: zhshgu436@163.com (Y. Zhang), jiayanlin@126.com (Y. Jia).
https://doi.org/10.1016/j.jmrt.2020.03.051

fine grain strengthening, which indicates the complicated process, low production efficiency, and product with limited size [4–6]. Therefore, in this work we looked forward to an easier process that involves low cost elements and multiple dispersion strengthening to meet increasingly urgent demand of high speed railway development.

It is noteworthy to mention that the nanoscale precipitates play an important role in strengthening materials. Especially, when there exists a complete coherent or semi-coherent interface structure between the matrix and the precipitates [7,8]. Gorsse et al. [9] confirmed that Cu-Mg alloy represent excellent mechanical properties with the precipitation of Cu_2Mg secondary phase. Lei et al. [10] proved that high strength of the Cu-Ni-Si alloy was attributed to the Orowan precipitation strengthening caused by the secondary phase. Mu at al. [11] investigated the aging behavior of the Cu-Cr-Zr-Mg-RE alloy and proved that zirconium-rich phase and the $CrCu_2$ particles caused good combination of the physical and mechanical properties. Zhang at al. [12] confirmed the Y_2O_3 oxide in the Cu-Mg-Te-Y alloy, which caused purification function and increased the tensile strength. Ren at al. [13,14] proved that trace Y cannot only markedly improve the alloys strength and ductility, but also have a good effect on the heat-resistance. Bu et al. [15] demonstrated that ultimate tensile strength and elongation of as-cast alloys increase with the addition of Y.

Alloy elements as pure Cu, Mg, Fe, Sn, P, and Y are introduced into Cu-Mg alloy in the experiment. Previous research [16] has proved that Mg element ranging from 0.3–1.0% (mass fraction) is normally applied in processing conductive wire. Trace Mg can cause decrease conductivity of Cu and increase the ability of Cu that resist oxidation at high temperature. Fe is rarely soluble in Cu with solubility of 0.15% at 635 °C, which can notably refine grain, delay recrystallization and improve the tensile strength of material. For P element, it can enhance the fluidity of copper matrix. Although introduction of P can decrease both electrical conductivity and thermal working properties of Cu-based alloy, it is beneficial for the mechanical and welding property. Especially, the precipitation of Mg_3P_2 phase formed by Mg and P eliminates the ability of two solid atoms to scatter electrons and improved the electrical conductivity.

Usually, the combination of cold deformation and aging processes is used to prepare nanoscale precipitation strengthening alloys. It is generally known that cold deformation can cause a large number of deformation twins and dislocations, which greatly improves the strength. However, the increase of strength is often accompanied by the decrease of material plasticity. A great deal of research reports has shown that aging treatment can effectively eliminate this phenomenon [17,18]. Thus, micro-alloying method (Mg, Fe, and P elements), cold deformation and aging treatment were used in this work, and the strengthening mechanism of the Cu-Mg-Fe-Sn-P-Y alloy was investigated.

2. Materials and methods

2.1. Preparation of specimens

Alloy ingots were prepared by induction melting of purified Cu, Mg, Sn, Y, master alloys Cu-10%Fe and Cu-12%P using a ZG-0.01 vacuum medium frequency induction melting furnace in an argon atmosphere at 1200 °C ± 10 °C and left to solidify at room temperature. The ingots with the total weight of 8 ± 0.5 kg were homogenized at 900 °C for 3 h and then extruded to the into a Φ35 mm cylinders by using the XJ-500 metal profile extrusion machine. Solution treatment was performed by the box-type resistance furnace (KSS-1200) at 900 °C for 2 h and then water quenched. The cylinders were machined into the sheets with a geometry of 100 mm × 5 mm × 1 mm. Then after 60% cold deformation the samples were aged at 460 °C for 10 min, 20 min, 30 min, 60 min, 120 min, 240 min, 360 min and 480 min.

2.2. Properties testing and microstructural characterization

Vickers hardness before and after aging treatment was measured at least 10 times using the HVS-1000 hardness tester to obtain the average value. The load was 100 g applied for 15 s with the ±5% measurement error. Resistivity of the samples was measured using the ZY9987 digital micro-ohm meter. Each sample was measured more than 3 times to obtain the average value within ±5% measurement error. According to the GB/T228-2002 standard, tensile properties of the studied alloy were tested using the AG-I 250 KN machine with a speed of 5.0 mm/min at room temperature. Three tension specimens under the same test conditions were tested separately. The error was less than ±3%. Energy dispersive spectroscopy (EDS) maps were acquired using a JSM-7800 F field emission scanning electron microscope. Thin foils with 3 mm diameter and 50 μm thickness for TEM and HRTEM analysis were electropolished by a DJ2000 twin-jet unit with a current of 73 mA and a temperature of around −35 °C using a mixed solution of HNO_3 and C_2H_5OH (mixed ratio of 1:4). Subsequently, the sample was cleaned with alcohol. Then the sample was ion thinning using a Gatan 691 iron beam thinner for around 30 min and the observations were conducted on a JEM-2100 transmission electron microscope.

3. Results

The low magnification BSE-SEM and the corresponding high magnification images of the Cu-Mg-Fe-Sn-P-Y alloy after extrusion at 900 °C are shown in Fig. 1a and b respectively. The matrix structure shows the obvious lamellar structure at high magnification. The elemental STEM-EDS maps of the boxed region Fig. 1b showing uniform distribution of all the principal elements. In addition, no other elements were found in EDS analysis, indicating that no impurities were added to the alloy during melting and high temperature extrusion. The composition analysis is shown in Table 1.

3.1. Properties

Fig. 2 shows the variation of hardness of the Cu-Mg-Fe-Sn-P-Y alloy with 60% cold deformation aged at 460 °C. The hardness increased significantly until 20 min, and then reached a plateau value between 20 min and 30 min. Afterwards, the hardness decreases gradually with the increase of aging time

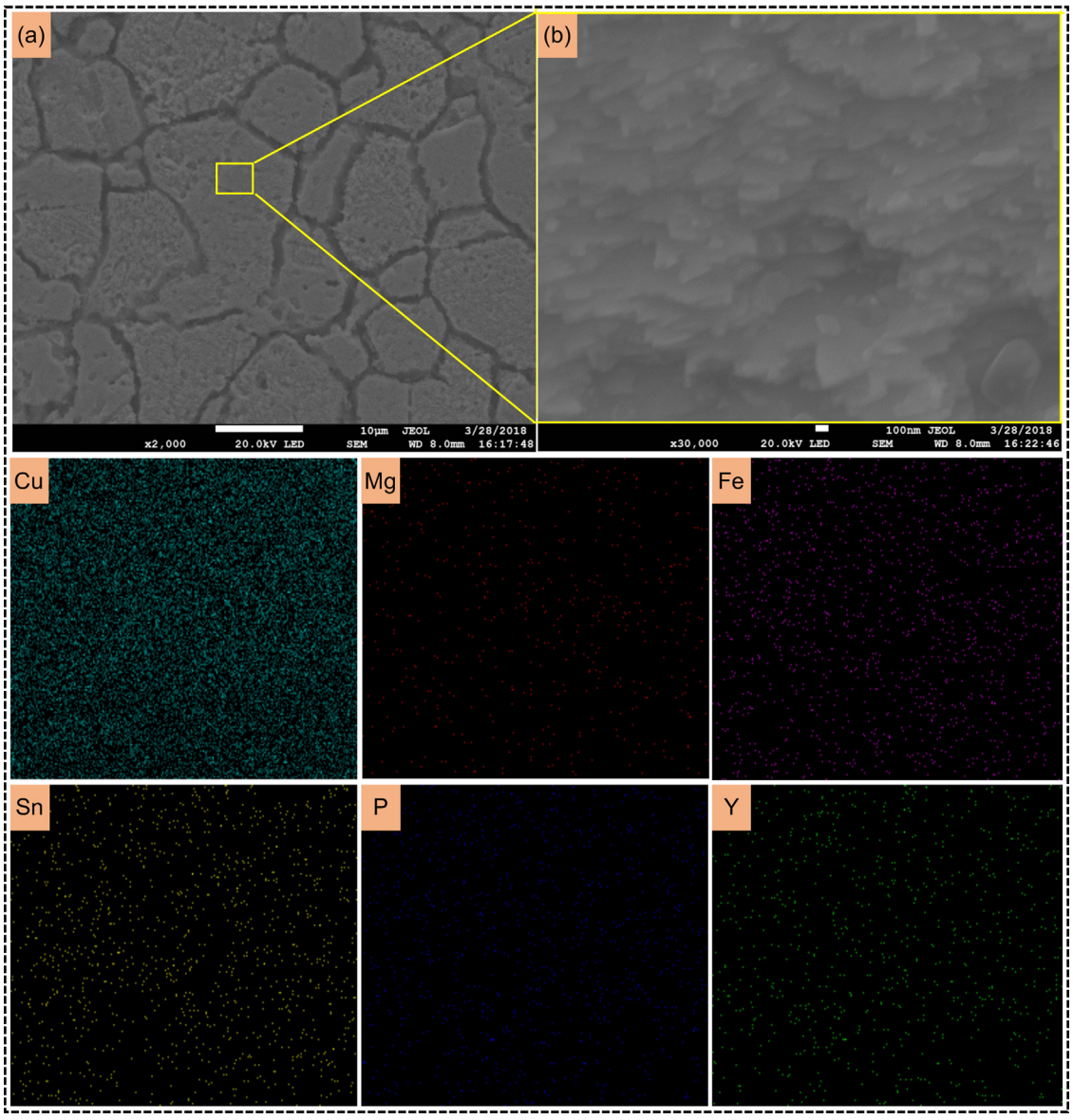

Fig. 1 – (a) low magnification BSE-SEM image; (b) corresponding high magnification image of the framed area in (a) and corresponding elemental STEM-EDS maps of Cu, Mg, Fe, Sn, P, and Y after high temperature extrusion, respectively.

(over-aging stage). Variation of the electrical conductivity is similar to the hardness (but kept stable instead of decreasing in the over-aging stage). At the beginning of aging, the precipitates has a faster precipitation rate and the scattering effect of solid solution atoms on electrons is weak. Thus, the conductivity increases rapidly. Later, the precipitates were continuously precipitated from the matrix and grew up gradually. At the over-aging stage, the precipitates precipitated completely from the matrix and the conductivity remained stable. Specifically, the alloy aged for 20 min exhibits the best comprehensive performance with the hardness of 179 HV and electrical conductivity of 71.1%IACS. The general explanation for variation of hardness is due to the growth of precipitates in the aging process [19,20]. The hardness increases at the under-aging stage, and then decreases as the precipitates grow up at the over-aging stage. In order to investigate the evolution of the precipitates, the aging time of 10 min, 20 min, 60 min, and 480 min were chosen to represent the conditions

Table 1 – Alloy compositions analysis.

Nominal composition (wt. %)	Analyzed composition (wt. %)				
	Mg	Fe	Sn	P	Y
Cu-0.4 Mg-0.2Fe-0.2Sn-0.15P-0.15Y	0.406	0.194	0.188	0.146	0.159

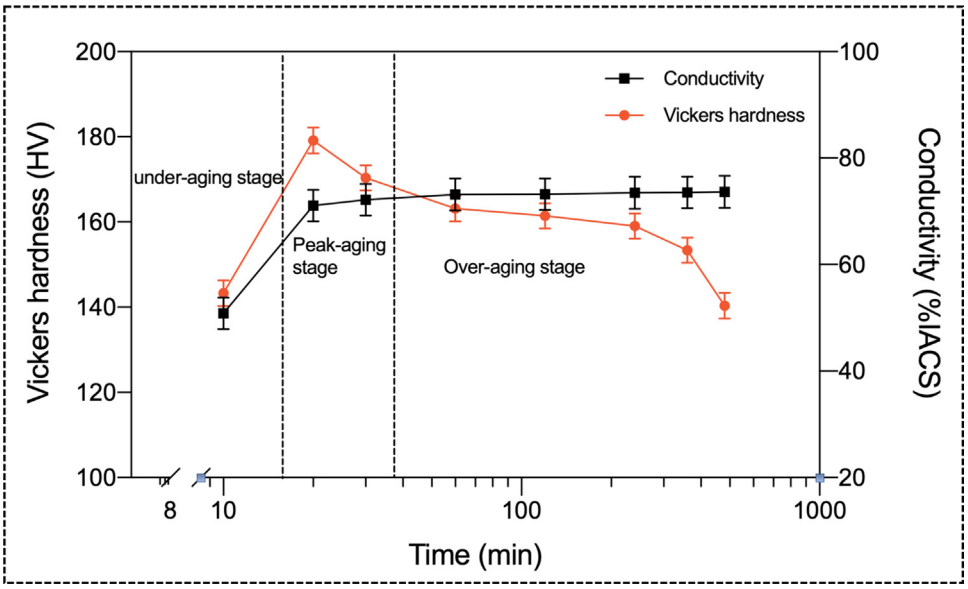

Fig. 2 – Variation of Vickers hardness and electrical conductivity with aging time of the Cu-Mg-Fe-Sn-P-Y alloy with 60% cold deformation aged at 460 °C.

of under-aging, peak-aging, and over-aging stages, respectively.

3.2. *Evolution of precipitates*

The bright-field TEM images of the Cu-Mg-Fe-Sn-P-Y alloy aged for 10 min (under-aging stage) and 20 min (peak-aging stage) are shown in Fig. 3a and c, respectively. The corresponding dark-field TEM images are shown in Fig. 3b and d, respectively. As shown in Fig. 3a, ultrafine precipitates (~3 nm) are uniformly distributed in the matrix for the 10 min aging. The nanoscale precipitates exhibit excellent dispersion strengthening effect. Therefore, the hardness increases significantly in the under-aging stage.

Then, at the peak-aging stage, precipitates in Fig. 3c present the petal shape. There is a non-contrast line between the particles and the direction of the non-contrast line is perpendicular to the Bragg reflection vector, which is a conformal strain contrast. According to the Cu-Fe phase diagram [21], it can be inferred that the precipitates in this experiment may be γ-Fe. Fig. 3e is the HRTEM image of Fig. 3c. The FFT pattern and inversed FFT image of the selected area a_1 were shown in Fig. 3f and g, respectively. The FFT pattern and inversed FFT image of the selected area a_2 (Cu matrix) were shown in Fig. 3h and i, respectively.

From Fig. 3f, it can be seen that the speckles of precipitated phase in a_1 and the matrix almost coincide, but the stress field appears in Fig. 3g. Besides, periodic dislocations appear at the interface between precipitates and the matrix marked by the T symbol, which is quite different from the Fig. 3i of the matrix without any dislocations. The dislocations with high density at the interface play an important role in strengthening Cu composites. This means that there is internal stress between the precipitated phase and the matrix, which is beneficial for improving the adhesion of the interface. Based on the prior reports [22], the lattice constants of Cu and γ-Fe are 0.360 and 0.362 nm, respectively. The mismatch between the Cu matrix and the γ-Fe precipitate is calculated as [21,23]:

$$\sigma = \frac{d_1 - d_2}{d_1} \quad (1)$$

Here σ is the mismatch of the precipitate and the matrix; d_1 is the interplanar spacing of the matrix, d_2 is the interplanar spacing of the precipitate. The mismatch of the two phases is 1%, which indicates the complete coherent relationship between the matrix and the precipitates. Therefore, the precipitate is identified to be fcc γ-Fe. The role of the nanoscale γ-Fe is that it can improve the strength according to pinning of dislocations and inhibiting movement of the grain boundaries, and leading to the occurrence of peak-aging stage. In addition, twins structure caused by cold deformation is shown in Fig. 3j, which causes an increase of subgrain boundaries and impacts the hardness performance.

In the initial over-aging stage, the bright-filed image of 60 min aging is shown in Fig. 4. In Fig. 4a, nanoparticles are uniformly distributed in the matrix. Different from the γ-Fe in Fig. 4c, dislocations appear around the precipitates, which indicates stress release. The dislocations bypassing particles and producing dislocation loops were observed in Fig. 4a, marked by red arrows, which is a typical Orowan strengthening mechanism. The reason is that the nanoparticles have high strength and hardness, and it is hard for dislocation lines to cut though. Consequently, the precipitates promote the proliferation of dislocations. When the dislocation lines continue circumventing the particles and moving, the number of the dislocation loops increases and effective spacing of particles decreases, resulting in enhancement of the effect. The dislocations are blocked by particles and show an arched shape, which is marked by the green circle with letter A in Fig. 4a.

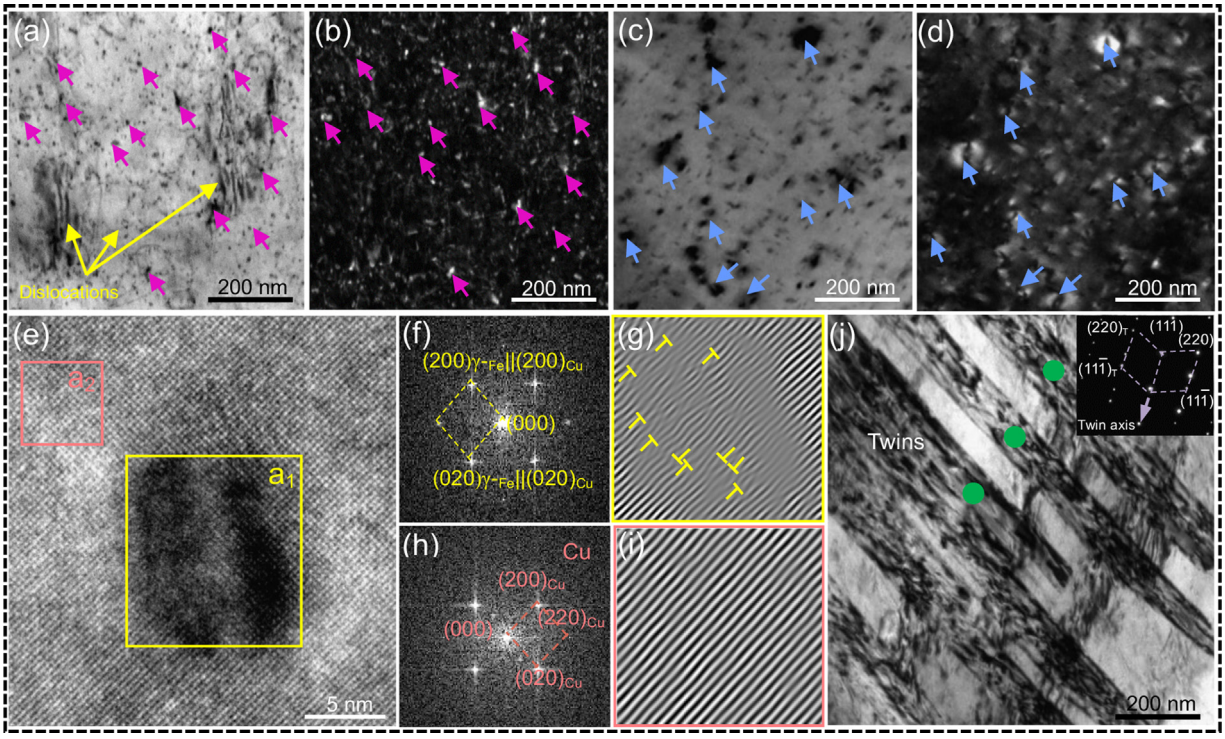

Fig. 3 – TEM images of the Cu-Mg-Fe-Sn-P-Y alloy with 60% cold deformation aged at 460 °C (a) 10 min; (b) dark-field TEM image of (a); (c) 20 min; (d) dark-field TEM image of (c); (e) HRTEM image taken from (b); (f) FFT pattern of the a1 framed region in (e); (g) inversed FFT images of (f) masking $(200)_{Cu}$ and $(200)_{\gamma\text{-Fe}}$ spots; (h) FFT pattern of the a_2 framed region in (e); (i) inversed FFT image of (i) masking $(020)_{Cu}$ and $(200)_{Cu}$ spots; (j) twins structure for 20 min.

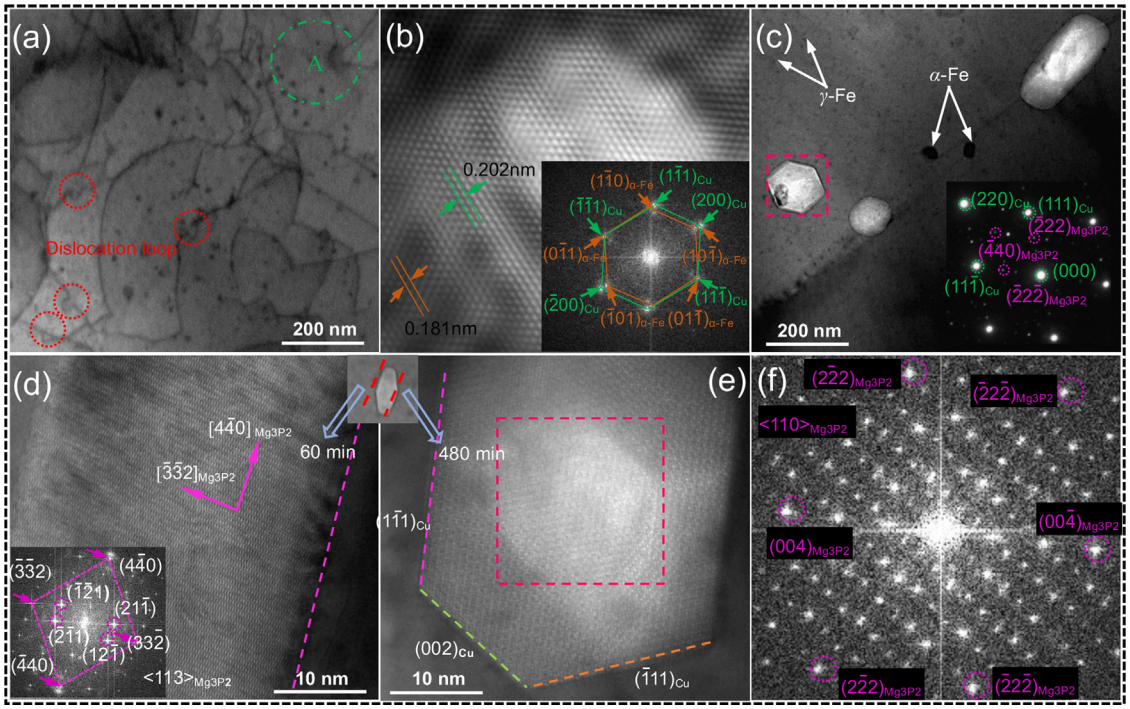

Fig. 4 – TEM images of the Cu-Mg-Fe-Sn-P-Y alloy with 60% cold deformation aged at 460 °C (a) bright-field image for 60 min; (b) inversed FFT image of the precipitate in the green circle in (a) masking $(200)_{Cu}$ and $(110)_{Fe}$ spots; (c) bright-field image for 480 min; (d) HRTEM image of 60 min; (e) HRTEM image of the red framed area in (c); (f) FFT pattern of the red framed area in (e).

In order to clarify the interfacial relationship between precipitates and the matrix, the HRTEM image of the nanoparticle in Fig. 4a was obtained. Fig. 4b shows the FFT pattern of precipitate in the green circle in Fig. 4a and the nanoparticle is determined to be bcc α-Fe viewed along the zone axis of $<011>_{Cu}$. This indicates that a part of γ-Fe lose the complete coherent relationship with the Cu matrix and formed α-Fe. It can be seen from the FFT pattern that $(\bar{1}\bar{1}1)_{Cu}//(0\bar{1}1)_{\alpha-Fe}$, $[0\bar{1}\bar{1}]_{Cu}//[\bar{1}\bar{1}\bar{1}]_{\alpha-Fe}$, which indicates that there is Nishiyama relationship between $(\bar{1}\bar{1}1)_{Cu}$ plane and $(0\bar{1}1)_{\alpha-Fe}$ plane. Meanwhile, the interplanar spacing of the $(200)_{Cu}$ plane and $(10\bar{1})_{\alpha-Fe}$ plane are 0.181 nm and 0.202 nm, respectively. The mismatch degree between $(200)_{Cu}$ plane and $(10\bar{1})_{\alpha-Fe}$ plane is calculated as 11.6%. Therefore, there is semi-coherent relationship between $(200)_{Cu}$ plane and $(10\bar{1})_{\alpha-Fe}$. Thus, the main reason for the decrease of hardness in the over-aging process is that γ-Fe transform to α-Fe, which is semi-coherent to the matrix. It is noteworthy that Mg_3P_2 precipitates were observed in this experiment. It is vary from the Cu_2Mg precipitates in previous studies [24,25]. Fig. 4c shows the bright-filed image of 480 min. The corresponding HRTEM images and FFT patterns of the alloy aged at 60 min and 480 min are shown in Fig. 4d and e, respectively. Fig. 4f shows the FFT pattern of Fig. 4e and the Mg_3P_2 (~114 nm) as orthogonal structure belonging to the Ia-3 space group, $a=b=c=12.03$ Å, $\alpha=\beta=\gamma=90^{\circ}$, zone axis of [110]Cu. Compared with Fig. 4d, the Mg_3P_2 has the definite orientation relationship (OR) of cubic to cubic with the Cu matrix after 480 min aging, $<110>_{Cu}||<110>_{Mg3P2}$, $(002)_{Cu}||(008)_{Mg3P2}$, which was rarely reported in similar investigations so far. The Mg_3P_2 greatly affects the alloy properties. It has been proved that the addition of Mg and P decreases the conductivity of copper alloy. However, the appearance of Mg_3P_2 greatly reduces the scattering effect of Mg and P solid solution atoms on electrons. Kim et al. [26] observed coarse Fe_3P at grain boundaries in Cu-Fe-P alloy and caused hardness decreased. However, in our opinion, the Mg_3P_2 hindered the appearance of coarse Fe_3P. The aggregation of Mg_3P_2 at grain boundaries not only reduces the effect of grain boundaries on conductivity, but also improves the alloy strength and hardness.

4. Discussion

4.1. *Orowan strengthening of the peak-aging stage*

The strength of the Cu-Mg-Fe-Sn-P-Y alloys is determined by the superposition of several strengthening mechanisms: strengthening caused by annealed pure copper (τ_a), precipitation hardening (τ_p), deforamtion hardening (τ_d), and the solid solution hardening (τ_s):

$$\tau = \tau_a + \Delta\tau_p + \Delta\tau_d + \Delta\tau_s \quad (2)$$

Here, $\tau_a = 272$ MPa, deformation strengthening was calculated by Ren et al. [27] in the Cu-Fe alloy. Therefore, the deformation strengthening is calculated as $\Delta\tau_d = 55$ MPa according to the same method. The precipitation strengthening ($\Delta\tau_p$) can be defined as the Orowan-Ashby equation [27,28]:

$$\Delta\tau_p = \frac{0.81\mu b}{2\pi(1-\upsilon)^{0.5}} \cdot \frac{\ln(2r_s/r_0)}{(l_s - 2r_s)} \quad (3)$$

Here μ is the shear modulus of the particles (5×10^4 MPa for Cu); b is the Burger vector (0.2556 nm for Cu); r_0 is the radius of the nucleus of the precipitate staggered region ($r_0 = b$); υ is the Poisson's ratio of the copper matrix ($\upsilon = 0.3$); r_s is the radius of precipitate; l_s is the inter-particle spacing. $r_s = 10$ nm, $l_s = 30$ nm, the strength increment caused by the Orowan strengthening mechanism of the alloy is calculated as $\Delta\tau_p = 352$ MPa. Therefore, relying on the ultimate tensile strength of the Cu-Mg-Fe-Sn-P-Y alloy aged at 460 °C and 20 min with the value of 599 MPa (as shown in Fig. 5a), has solution strengthening $\Delta\tau_s = 599–352-272-55 = 80$ MPa. The ratios of precipitation strengthening, deformation strengthening and solution strengthening are 58%, 9%, and 15%, respectively. According to the above analysis and calculations, it can be concluded that precipitation strengthening is the main strengthening mechanism in the aging process of the investigated alloy.

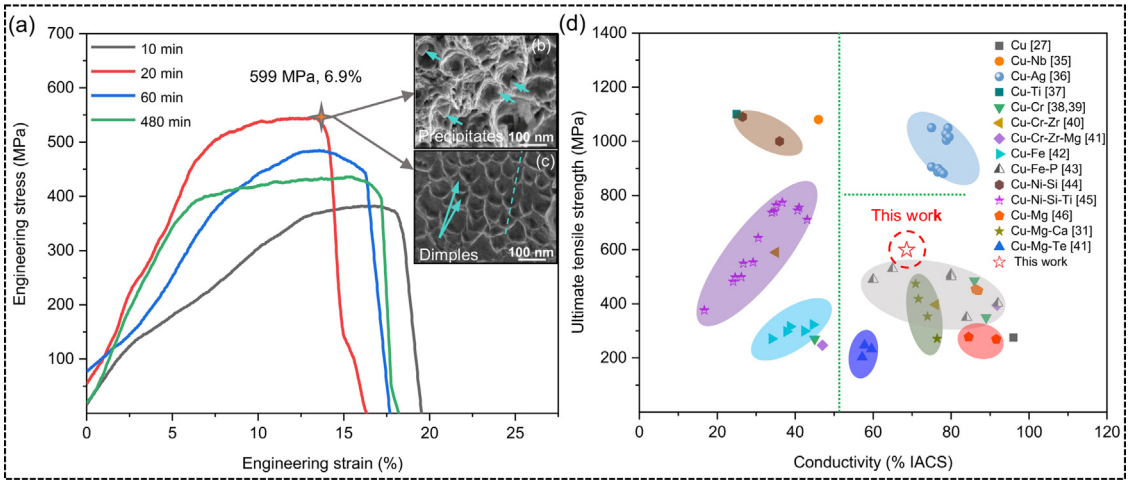

Fig. 5 – (a) tensile engineering stress-strain curves under for Cu-Mg-Fe-Sn-P-Y alloy with 60% cold deformation aged at 460 °C; (b) and (c) the corresponding fracture morphology of the studied alloy aged at 20 min in (a); (d) comparison of ultimate tensile strength and conductivity of Cu-based alloys.

4.2. *Property comparison*

Fig. 5a shows variation of tensile stress-strain curves of the Cu-Mg-Fe-Sn-P-Y alloy with 60% cold deformation aged at 460 °C. Maximum tensile strength occurs after 20 min aging with 6.9% elongation and 599 MPa tensile strength. The corresponding fracture images (peak-aging state) are shown in Fig. 5b and c. This is a typical ductile fracture. The dimples are relatively developed and have a certain fracture orientation (marked by blue dashed line), which indicates that the material has high tensile strength and ductility [29–32]. The deep dimple and quasi-cleavage fracture appeared. In addition, it can be seen from Fig. 5c that there are no cracks terminate near the nanoscale precipitates, implying that the precipitates play an important role in strengthening [33,34]. In order to improve the evaluation of the properties for the tested alloys, the properties of main electrical contact wires in recent years [12,27,31,35–46] are summarized in Fig. 5d. It can be seen that the Cu-Ni-Si alloy has higher tensile strength, but lower electrical conductivity. The comprehensive properties of Cu-Ag alloy are better, but the cost of Ag is higher, so it is not suitable for industrial production. In view of the performance and economic cost, the Cu-Mg-Fe-Sn-P-Y alloy of 60% cold deformation aged at 460 °C for 20 min can satisfy the demand for tensile strength (500 MPa), electrical conductivity (62%IACS) and elongation (3–10%) at speeds above 400 km/h for the CTMM150 of China contact wires in TB/T 2809-2005 [1]. The ultimate tensile strength (599 MPa) and electrical conductivity (71.1%IACS) increased by 20% and 15%, respectively. As a result, this work can replace the current Cu-Mg, Cu-Ag, and Cu-Sn electrical contact wires above 400 km/h of the high speed railway.

5. Conclusions

In summary, we mainly concentrated on the evolution of the precipitates and their effects on the alloy properties via aging treatment. Meanwhile, it has been proven that the ultimate strength and hardness of the material are greatly improved because of the OR between the matrix and the nanoparticles. The main precipitate γ-Fe transformed to α-Fe at over-aging stage. The Mg_3P_2 phase hindered the appearance of coarse Fe_3P and improved the electrical conductivity and mechanical property the materials. Precipitation strengthening is the main strengthening mechanism in the aging process of the investigated alloy. The optimal aging parameter for Cu-Mg-Fe-Sn-P-Y alloy is 60% cold deformation and aged at 460 °C for 20 min with the high tensile strength of 599 MPa, conductivity of 71.1%IACS, and the elongation of 6.9%. Compared with current electrical contact wires, the ultimate tensile strength and conductivity of the Cu-Mg-Fe-Sn-P-Y alloy increased by 20% and 15%, respectively. The studied alloy has better comprehensive properties for industrial production.

Conflicts of interest

The authors declare no conflicts of interest.

Acknowledgements

This work was supported by the National Natural Science Foundation of China (U1704143) and the Open Cooperation Project of Science and Technology of the Hennan Province (172106000058 and 182106000018). This work was also supported by the National Science Foundation (IRES 1358088), USA.

REFERENCES

[1] Zhen G, Kim Y, Chuang LH, Koo JM, Seok CS, Lee K, et al. Bending fatigue life evaluation of Cu-Mg alloy contact wire. Int J Precis Eng Man 2014;15:1331–5.
[2] Purcek G, Saray O, Kul O, Karaman I, Yapici GG, Haouaoui M, et al. Mechanical and wear properties of ultrafine-grained pure Ti produced by multi-pass equal-channel angular extrusion. Mater Sci Eng A 2009;517:97–104.
[3] Yang G, Li Z, Yuan YY, Lei Q. Microstructure, mechanical properties and electrical conductivity of Cu-0.3Mg-0.05Ce alloy processed by equal channel angular pressing and subsequent annealing. J Alloys Compd 2015;640:347–54.
[4] An XH, Wu SD, Zhang ZF, Figueiredo RB, Gao N, Langdon TG. Enhanced strength-ductility synergy in nanostructured Cu and Cu-Al alloys processed by high-pressure torsion and subsequent annealing. Scr Mater 2012;66:227–30.
[5] Saray O, Purcek G, Karaman I, Neindorf T, Maier HJ. Equal-channel angular sheet extrusion of interstitial-free (IF) steel: Microstructural evolution and mechanical properties. Mater Sci Eng A 2011;528:6573–83.
[6] Velasco L, Polyakov MN, Hodge AM. Influence of stacking fault energy on twin spacing of Cu and Cu-Al alloys. Scr Mater 2014;83:33–6.
[7] Stanford N. Micro-alloying Mg with Y, Ce, Gd and La for texture modification – a comparative study. Mater Sci Eng A 2010;527:2669–77.
[8] Cheng JY, Tang BB, Yu FX, Shen B. Evaluation of nanoscaled precipitates in a Cu-Ni-Si-Cr alloy during aging. J Alloys Compd 2014;614:189–95.
[9] Gorsse S, Ouvrard B, Gouné M, Poulon-Quintin A. Microstructural design of new high conductivity-high strength Cu-based alloy. J Alloys Compd 2015;633:42–7.
[10] Lei Q, Xiao Z, Hu WP, Derbyb B, Li Z. Phase transformation behaviors and properties of a high strength Cu-Ni-Si alloy. Mater Sci Eng A 2017;697:37–47.
[11] Mu SG, Guo FA, Tang YQ, Cao XM, Tang MT. Study on microstructure and properties of aged Cu-Cr-Zr-Mg-RE alloy. Mater Sci Eng A 2008;475:235–40.
[12] Zhang XG, Han JN, Chen L, Zhou BW, Xue YY, Jia F. Effects of B and Y additions on the microstructure and properties of Cu-Mg-Te alloys. J Mater Res 2013;8:2747–52.
[13] Ren LB, Quan GF, Zhou MY, Guo YY, Jiang ZZ, Tang Q. Effect of Y addition on the aging hardening behavior and precipitation evolution of extruded Mg-Al-Zn alloys. Mater Sci Eng A 2017;690:195–207.
[14] Somekawa H, Osawa Y, Singh A, Washio K, Kato A, Mukai T. Effect of micro-alloying elements on deformation behavior in Mg-Y binary alloys. Mater Trans 2014;55:182–7.
[15] Bu FQ, Yang Q, Qiu X, Zheng T, Zhang DP, Niu XD, et al. Study on the assemblage of Y and Gd on microstructure and mechanical properties of hot extruded Mg-Al-Zn alloy. Mater Sci Eng A 2015;639:198–207.
[16] Kim SS, Rhu JC, Jung YC, Han SZ, Kim CJ. Aging characteristics of thermomechanically processed Cu-9Ni-6Sn alloy. Scr Mater 1998;40:1–6.

[17] Chino Y, Kimura K, Mabuchi M. Twinning behavior and deformation mechanisms of extruded AZ31 Mg alloy. Mater Sci Eng A 2008;486:481–8.
[18] Cheng JY, Yu FX, Shen B. Solute clusters and chemistry in a Cu-Cr-Zr-Mg alloy during the early stage of aging. Mater Lett 2014;115:201–4.
[19] Su JH, Dong QM, Liu P, He HJ, Kang BX. Research on aging precipitation in a Cu-Cr-Zr-Mg alloy. Mater Sci Eng A 2005;392:422–6.
[20] Varma VK, Mahajan YR, Kutumbarao VV. Ageing behaviour of Al-Cu-Mg alloy matrix composites with SiCp of varying sizes. Scr Mater 1997;37:485–9.
[21] Dong QY, Wang MP, Shen LN, Jia YL, Li Z. Diffraction analysis of α-Fe precipitates in a polycrystalline Cu-Fe alloy. Mater Charact 2015;105:129–35.
[22] Shi GD, Chen XH, Jiang H, Wang ZD, Tang H, Fan YQ. Strengthening mechanisms of Fe nanoparticles for singlecrystal Cu-Fe alloy. Mater Sci Eng A 2015;636:43–7.
[23] Hu T, Chen JH, Liu JZ, Liu ZR, Wu CL. The crystallographic and morphological evolution of the strengthening precipitates in Cu-Ni-Si alloys. Acta Mater 2013;61:1210–9.
[24] Wang BJ, Zhang Y, Tian BH, Yakubov V, An JC, Volinsky AA, et al. Effects of Ce and Y addition on microstructure evolution and precipitation of Cu-Mg alloy hot deformation. J Alloys Compd 2019;781:118–30.
[25] Godbole RP, Jha SA, Milanarun M, Mishra AK. Thermodynamics of liquid Cu-Mg alloys. J Alloys Compd 2004;363:187–93.
[26] Kim HG, Lee TW, Han SZ, Euh K, Kim WY, Lim SH. Microstructural study on effects of C-alloying on Cu-Fe-P cast alloy. Met Mater Inter 2012;18:335–9.
[27] Ren FZ, Wang J, Ma ZH, Su JH, Jia SG. Properties of Cu and Fe under large deformation and strength calculation of Cu-11.5%Fe in sit composites. Mater Heat Treat 2009;30:15–9.
[28] Mohamed IF, Yonenaga Y, Lee S, Edalati K, Horita Z. Age hardening and thermal stability of Al-Cu alloy processed by high-pressure torsion. Mater Sci Eng A 2015;627:111–8.
[29] Sauvage X, Bobruk EV, Murashkin MY, Nasedkina Y, Enikeev NA, Valiev RZ. Optimization of electrical conductivity and strength combination by structure design at the nanoscale in Al-Mg-Si alloys. Acta Mater 2015;98:355–66.
[30] Bao GH, Xu YQ, Huang LY, Lu XP, Zhang L, Fang YT, et al. Strengthening effect of Ag precipitates in Cu-Ag alloys: a quantitative approach. Mater Res Lett 2016;4:37–42.
[31] Li YP, Xiao Z, Li Z, Zhou ZY, Yang ZQ, Lei Q. Microstructure and properties of a novel Cu-Mg-Ca alloy with high strength and high electrical conductivity. J Alloys Compd 2017;723:1162–70.
[32] Raju KS, Sarma VS, Kauffmann A, Hegedus Z, Gubicza J, Peterlechner M, et al. High strength and ductile ultrafine-grained Cu-Ag alloy through bimodal grain size, dislocation density and solute distribution. Acta Mater 2013;61:228–38.
[33] Kamat SV, Gogla AK, Banerjee D. Effect of alloying elements and heat treatment on the fracture toughness of Ti-Al-Nb alloys. Acta Mater 1998;46:239–51.
[34] Murthy AS, Medvedeva JE, Isheim D, Lekakh SL, Richards VL, Aken DCV. Copper precipitation in cobalt-alloyed precipitation-hardened stainless steel. Scr Mater 2012;66:943–6.
[35] Mattissen D, Raabe D, Heringhaus F. Experimental investigation and modeling of the influence of microstructure on the resistive conductivity of a Cu-Ag-Nb in situ composite. Acta Mater 1997;47:1627–34.
[36] Sakai Y, Inoue K, Madae H. New high-strength, high-conductivity Cu-Ag alloy sheets. Acta metall Mater 1995;43:1517–22.
[37] Semboshi S, Takasugi T. Fabrication of high-strength and high-conductivity Cu-Ti alloy wire by aging in a hydrogen atmosphere. J Alloys Compd 2013;580:S397–400.
[38] Vinogradov A, Ishida T, Kitagawa K, Kopylov VI. Effect of strain path on structure and mechanical behavior of ultra-fine grain Cu-Cr alloy produced by equal-channel angular pressing. Acta Mater 2005;53:2181–92.
[39] Kim JM, Park JS, Kim KT. Electrical conductivity and tensile properties of severely cold-worked Cu-P based alloy sheets. Met Mater Int 2010;16:657–61.
[40] Purcek G, Yanar H, Saray O, Karaman I, Maier HJ. Effect of precipitation on mechanical and wear properties of ultrafine-grained Cu-Cr-Zr alloy. Wear 2014;311:149–58.
[41] Gan CL, Liu H, Zheng KH, Liu N, Wang HY. Manufactured process of high strength and high electrical conductivity Cu-Cr-Zr-Mg alloy bars. Mater Sci Forum 2017;898:1215–9.
[42] Wei DQ, Shen LN, Cao F, Jia YL, Wang MP. Study of the coarsening and hardening behaviors of the coherent γ-Fe particles in Cu-201Fe alloy. Acta Metall Sin 2014;50:1224–30.
[43] Lu DP, Wang J, Zeng WJ, Liu Y, Lu L, Sun BD. Study on high-strength and high-conductivity Cu-Fe-P alloys. Mater Sci Eng A 2006;421:254–9.
[44] Lei Q, Li Z, Xiao T, Pang Y, Xiang ZQ, Qiu WT, et al. A new ultrahigh strength Cu-Ni-Si alloy. Intermetallics 2013;42:77–84.
[45] Lee E, Euh K, Han SZ, Lim S, Lee J, Kim SS. Tensile and electrical properties of direct aged Cu-Ni-Si-x%Ti alloys. Met Mater Int 2013;19:183–8.
[46] Zhu CC, Ma AB, Jiang JH, Li XB, Song D, Yang DH, et al. Effect of ECAP combined cold working on mechanical properties and electrical conductivity of conform-produced Cu-Mg alloys. J Alloys Compd 2014;582:135–40.